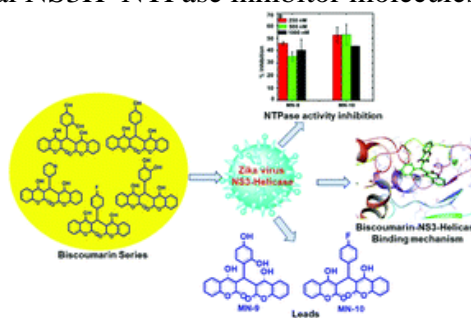| Sl. No.	**IIT Ropar** **List of Recent Publications with Abstract** **Coverage: January, 2020**
1.	A Cryogenic Front-End Preamplifier Operating at 120 K for Bolometric Detector A Reza, V Vatsa, MS Pose, A Mazumdar… RG Pillay… - Journal of Low Temperature Physics, 2020 **Abstract:** In this paper, the design and test results of a front-end cryogenic amplifier for a bolometer detector are presented. The amplifier is implemented with two low-noise Si JFETs, where the first FET is configured as a source follower amplifier and the second FET provides a high dynamic resistance to keep the voltage gain very close to unity. A 3 dB bandwidth over a wide range from DC to 10 MHz is achieved in this design. The input voltage noise density is ~ 1.9 nV/$\sqrt{\text{Hz}}$ at 300 K, which further reduces to 1.6 nV/$\sqrt{\text{Hz}}$ at 120 K. The flicker corner frequency observed is below 50 Hz.
2.	A Rapid Method of Determination of Swell Potential and Swell Pressure of Expansive Soils Using Constant Rate of Strain Apparatus TA Kumar, M Raheena, RG Robinson, T Thyagaraj - Geotechnical Testing Journal, 2020 **Abstract:** Swell potential and pressure of expansive soils are conventionally determined using an oedometer apparatus. The specimens are commonly saturated by submerging in water under a seating pressure. Generally, the test takes a long time, as the saturation process is slow. This article presents an improved saturation method by back pressure application in a constant rate of strain (CRS) loading apparatus. Controlled strain loading (CSL) was adopted to bring back the swollen specimens to their initial thickness instead of conventional incremental loading. It is observed that the time taken to complete the test is 7 to 13 times faster compared to the conventional method. When compared to the conventional method, the swell potential and pressure values obtained with the back pressure saturation were found to be higher by about 19 % to 34 % and 6 % to 28 %, respectively. The reason for these higher values is attributed to the attainment of greater saturation using the back pressure saturation technique.
3.	An efficient analytical model for microstrip spurline band-stop filter design S Agarwal, A Sharma - Microwave and Optical Technology Letters, 2020 **Abstract:** An efficient analytical model to design wideband microstrip spurline band-stop filter (BSF) is proposed. The geometrical parameters of the BSFs are optimized using simulation for the entire range of the desired operating frequency (1-5 GHz) and the results indicated relatively inferior performance of the filters designed using conventional analytical model. Whereas, in the proposed model, a mathematical function is found by curve fitting of the optimal data set of geometrical parameters optimized by simulation. Therefore, the filters designed using the proposed model achieve almost optimal performance in terms of rejection ratio, bandwidth, and so on, and a better match between desired and actual operating frequency as compared with the conventional design model. To corroborate the claims, the filter prototypes designed using the proposed and conventional models are fabricated and tested. The measured results showed agreement with the simulation results and proved effectiveness of the proposed analytical model to design spurline BSF. The error limit for the proposed model is found within ±0.005% of the optimal design.

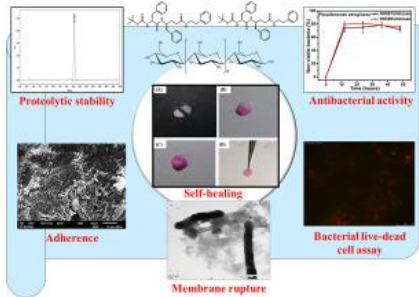|	
4.	[Biscoumarin scaffold as an efficient anti-Zika virus lead with NS3-Helicase inhibitory potential: in-vitro and in-silico Investigation](#) D Kumar, N Kaur, R Giri, N Singh - New Journal of Chemistry, 2020 **Abstract:** As a way to investigate new antiviral leads against Zika virus (ZIKV), we have targeted the NS3 helicase (NS3H) protein with biscoumarin derivatives. The NS3H protein from ZIKV is important, as it plays a significant role in the viral genome replication process. We have assessed the NTPase modulatory effects of biscoumarin derivatives against the NTPase activity of NS3H through in vitro enzymatic studies. Subsequently, to explore the mechanism, detailed computational studies were conducted. The NS3H protein has two binding cavities: one is the NTPase binding cavity where ATP binds, and the other is an RNA binding cavity for the binding of RNA molecules. Biscoumarin derivatives were found to be efficient in binding to both cavities, i.e., the NTPase and RNA binding cavities of the NS3H protein. A biscoumarin derivative with the best binding affinity for the NTPase binding cavity and the lowest binding affinity for the RNA binding groove revealed the best in vitro NTPase inhibitory activity. Also, the biscoumarin derivative with the lowest binding affinity for the NTPase binding cavity and higher binding affinity for the RNA binding cavity revealed the worst NTPase inhibitory activity under the same in vitro assay conditions. Here, we concluded that biscoumarin derivatives are modulators of the NS3H protein and they can be considered as promising anti-viral lead molecules. The structural activity relationships (SARs) of the biscoumarin derivatives in relation to their NTPase inhibitory activities were established, and we reported two derivatives, namely MN-9 and MN-10, as potential NS3H–NTPase inhibitor molecules.
5.	[Comparative assessment of different air-conditioning systems for nearly/net zero-energy buildings](#) G Singh, R Das - International Journal of Energy Research, 2020 **Abstract:** This study deals with the performance of different air-conditioning strategies for achieving the target of nearly/net zero energy in a medium-scale building under various environmental conditions. In particular, vapour compression (VC), vapour absorption (VA), and integration of radiant cooling technology are analysed using renewable energy resources emissions and solar photovoltaic (PV)-based electricity. Four different kinds of air-conditioning configurations are considered: VC-based, VA-based, VC-radiant air-conditioning technology with VC dedicated outdoor air system (DOAS) and VA radiant air-conditioning technology with VC-DOAS. Numerical model validations with the benchmark standards are done for VC- and VA-based systems. In particular, annual electric consumption, electricity generation, thermal load generation among all configurations, emissions and solar fractions are studied. The present study shows that target of nearly/net zero-energy building can be achieved in an efficient manner through radiant VC-based system with VC-DOAS for hot-dry and composite (ie, hot-dry

with higher humidity) environment conditions. However, for warm-humid environment, complete net zero is not possible, but up to 74% of net zero target can be assured with VC-based radiant and DOAS. With respect to the conventional VC-based system, the payback period assessment for the most suitable nearly/net zero building cooling system varies in the range of 5-9 years, depending on the environmental conditions.

| 6. | Design, characterization, and evaluation of antibacterial gels, Boc-D-Phe-γ4-L-Phe-PEA/chitosan and Boc-L-Phe-γ4-L-Phe-PEA/chitosan, for biomaterial-related infections
K Malhotra, S Shankar, N Chauhan, R Rai, Y Singh - Materials Science and Engineering: C, 2020 |

Abstract: Self-assembled peptide gels have generated interest as antibacterial materials to prevent biomaterial-related infections but these peptides are often associated with poor proteolytic stability. Efforts have been made to stabilize peptides by incorporating non-natural amino acids and/or linkages but complexation with polymers have not been explored. Therefore, we developed self-assembled peptide/chitosan gels, Boc-D-Phe-γ4-L-Phe-PEA (NH007)/chitosan and Boc-L-Phe-γ4-L-Phe-PEA (NH009)/chitosan, by complexing dipeptide NH007 or NH009 with chitosan in DMSO:acetic acid. The gels were characterized using SEM, FTIR, contact angle, and rheology data and found to exhibit excellent viscoelastic and self-healing characteristics. Complexation with chitosan led to an increase in stability against proteolytic degradation. Peptide/chitosan gels showed broad spectrum antibacterial activities against Gram-negative and Gram-positive bacteria, such as Escherichia coli, Pseudomonas aeruginosa, Staphylococcus aureus, and Bacillus subtilis at a high inoculum of 10^7–10^8 cfu/mL. NH007/chitosan gels showed 70–75% inhibition, whereas NH009/chitosan showed 78–81% inhibition and NH009/chitosan gels, in particular, showed strong antibacterial activity against pathogenic strain of P. aeruginosa. A unique feature of these gels is that the antibacterial activities did not decrease gradually but were sustained for up to 48 h. The mechanistic studies using SEM and HR-TEM indicated interaction of gels with bacterial membrane components, leading to cell lysis. The MTT and LDH assays indicated >90% cell viability and only 8–10% toxicity towards NIH 3T3 fibroblast cells. Thus, peptide/chitosan gels developed in the present work showed improved proteolytic stability and sustained antibacterial activities and, therefore, may be used for preventing biomaterial-related infections.

Graphical Abstract:

| 7. | Determination of Range of Fuel Premixing Ratio in Compression Ignition Engine for Lower Exhaust Emissions and Higher Efficiency
MR Saxena, RK Maurya - SAE Technical Paper, 2020 |

Abstract: In this study, the influence of fuel premixing ratio (PMR) on the performance, combustion and emission characteristics of dual fuel operation in compression ignition (CI)
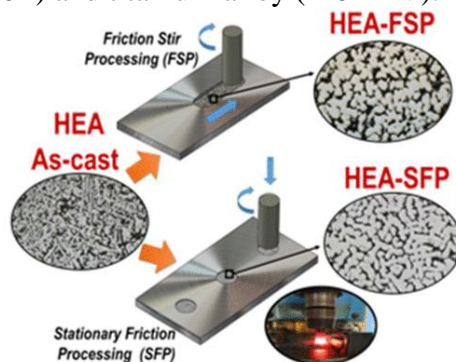
	engine has been investigated. For dual fuel operation in CI-engine, two fuels of different reactivity are utilized in the same combustion cycle. In this study, low reactivity fuels such as gasoline/butanol is injected into the intake manifold and high reactivity fuel (diesel) is directly injected into the cylinder. To operate the conventional CI engine in dual fuel mode, the intake manifold of the engine was modified and a solenoid based port fuel injector was installed. A separate port fuel injector controller was used for injecting the gasoline/butanol. Suitable instrumentation was used to measure the in-cylinder pressure and exhaust gas emissions. Experiments were performed by maintaining the constant fuel energy at different fuel PMR for different engine loads at constant engine speed. The influence of fuel PMR on combustion pressure, heat release rate, and coefficient of variance (COV) in indicated mean effective pressure (IMEP), brake thermal efficiency (BTE), combustion duration, and gaseous emissions were investigated at different engine loads. The main objective of present study is to determine the range of fuel PMR and best possible fuel PMR for gasoline/butanol-diesel dual fuel CI-engine at 25%, 50% and 100% loads. Additionally, butanol-diesel dual fuel operation is also compared with gasoline-diesel dual fuel operation for 50% engine load. The range of fuel PMR is estimated on the basis of combustion (COV of IMEP) and unburned hydrocarbon (HC) emission characteristics while best fuel premixing ratio is estimated on the basis of performance and emissions characteristics. The results demonstrate that higher thermal efficiency was achieved for specific combinations of fuel premixing ratio and NOx emission drastically reduced for both the dual fuel operations. Particle number emissions are also found lower in dual fuel operation (using gasoline and butanol) in the determined range of premixing ratio.
8.	Does financial literacy affect the value of financial advice? A contingent valuation approach Y Chauhan, DK Dey - Journal of Behavioral and Experimental Finance, 2020 **Abstract:** The paper examines the determinants of investors' willingness to pay (WTP) for suitable advice. We use contingent valuation, a method frequently used to estimate the value of non-market goods and services, with a unique survey data to estimate WTP for suitable advice. We find that investors with a high level of financial literacy recognize the value of financial advice; therefore, they have a higher WTP. These investors are also less likely to consult with a financial adviser if the advisory fee exceeds investors' maximum WTP. We also suggest the policy implications of our empirical results.
9.	Energy Saving Potential of an Air-Conditioning System with Desiccant and Solar Assisted Ventilation G Singh, R Das - Advances in Mechanical Engineering, 2020 **Abstract:** In this paper, a simulation analysis has been performed using Energy Plus software on the conventional vapor compression-based building cooling system for warm-humid climate. In order to achieve an energy efficient approach, decoupling of latent and sensible heat loads is done using a separate desiccant-assisted dedicated outdoor air system (DOAS). A solar collector system is installed to provide the required amount of heating energy for regenerating the desiccant. Further, an integrated evaporative cooling (IEC) arrangement in DOAS is used to improve the system performance. The performance of the system is evaluated using three distinct modes of operation. Results show that in comparison with the conventional compression operated system, desiccant-assisted DOAS in conjunction with IEC system saves 2.62% of electrical energy on an annual basis.

10.	[Enhanced Bio-Corrosion Resistance and Cellular Response of Dual-Phase High Entropy Alloy through Reduced Elemental Heterogeneity](#) G Perumal, HS Grewal, M Pole, LVK Reddy…H Singh… - ACS Applied Bio Materials, 2020 **Abstract:** The leaching out of toxic elements from metallic bioimplants has serious repercussions, including allergies, peripheral neuritis, cancer, and Alzheimer's disease, leading to revision or replacement surgeries. The development of advanced structural materials with excellent biocompatibility and superior corrosion resistance in the physiological environment holds great significance. High entropy alloys (HEAs) with a huge compositional design space and outstanding mechanical and functional properties can be promising for bioimplant applications. However, microstructural heterogeneity arising from elemental segregation in these multiprinciple alloy systems is the Achilles heel in the development of next-generation HEAs. Here, we demonstrate a pathway to homogenize the microstructure of a biocompatible dual-phase HEA, comprising refractory elements, namely, MoNbTaTiZr, through severe surface deformation using stationary friction processing (SFP). The strain and temperature field during processing homogenized the elemental distribution, which was otherwise unresponsive to conventional annealing treatments. Nearly 15 min of the SFP treatment resulted in a significant elemental homogenization across dendritic and interdendritic regions, similar to a week-long annealing treatment at 1275 K. The SFP processed alloy showed a nearly six times higher biocorrosion resistance compared to its as-cast counterpart. X-ray photoelectron spectroscopy was used to investigate the nature of the oxide layer formed on the specimens. Superior corrosion behavior of the processed alloy was attributed to the formation of a stable passive layer with zirconium oxide as the primary constituent and higher hydrophobicity. Biocompatibility studies performed using the human mesenchymal stem cell line, showed higher viability for the processed HEA compared to its as-cast counterpart as well as conventional metallic biomaterials including stainless steel (SS316L) and titanium alloy (Ti6Al4V).
11.	[Estimation of refractive index profiles of vertically aligned disordered silicon nanowires for photon management applications](#) SK Saini, RV Nair - SPIE Micro+ Nano Materials, Devices, and Applications, Proceedings Volume 11201, 2019 **Abstract:** We discuss a promising method to assess the refractive index profile of vertically aligned disordered Silicon nanowire arrays. The aberration-free micro-reflectivity set-up equipped with an in-situ optical microscope is designed to measure the reflectivity from $4 \mu m^2$ area of the nanowires. The spatial- and polarization-dependent reflectivity values along the nanowire length is used to estimate the refractive index profile. The transfer matrix method

	involving the estimated refractive index profiles is employed to corroborate the measured reflectivity values. The disordered Silicon nanowires with gradient refractive index profile can suppress 96 % reflectivity irrespective of direction, wavelength, and polarization which make them a potential candidate for photon management applications.
12.	Experimental Investigation of Combustion Stability and Particle Emission from CNG/Diesel RCCI Engine MR Saxena, RK Maurya – SAE Technical Paper, 2020 **Abstract:** This paper presents the experimental investigation of combustion stability and nano-particle emissions from the CNG/diesel RCCI engine. A modified automotive diesel engine is used to operate in RCCI combustion mode. An open ECU is used to control the low and high reactivity fuel injection events. Engine tests are conducted for different engine speed and load conditions. The tests are performed for various port fuel injected CNG masses and diesel injection timing including single and double diesel injection strategy. Several consecutive engine cycles are recorded using in-cylinder combustion pressure measurement. Statistical as well as Wavelet transform techniques are used to investigate the combustion stability in CNG/diesel RCCI engine. Differential mobility spectrometer is used for the measurement of particle number concentration and particle-size number distribution. The results indicate that double injection strategy has relatively higher concentration of nucleation mode particles and increases with advancing the diesel injection timings. Double diesel injection results in to reduced cyclic combustion variations in comparison to double diesel injection strategy. Additionally, CO and THC emissions are increasing with advanced diesel injection timing and are relatively lower for double injection strategy.
13.	Flow of wormlike micellar solutions through a long micropore with step expansion and contraction C Sasmal - Physics of Fluids, 2020 **Abstract:** In this study, an extensive numerical investigation has been carried out in order to understand the flow characteristics of a wormlike micellar (WLM) solution through a long micropore with step expansion and contraction. The VCM (Vasquez-Cook-McKinley) [P. A. Vasquez, G. H. McKinley, and P. L. Cook, "A network scission model for wormlike micellar solutions: I. Model formulation and viscometric flow predictions," J. Non-Newtonian Fluid Mech. 144, 122–139 (2007)] constitutive model has been used for the present WLM solution for predicting its rheological behavior and the governing equations, namely, mass and momentum equations along with the VCM constitutive model equations have been solved using the finite-volume method based open source code OpenFOAM. Within the range of conditions encompassed in this study, different flow regimes have been observed in the pore geometry, for instance, Newtonian like regime, lip vortex formation regime, unsteady and vortex merging regime, etc. In particular, an elastic instability regime has been observed in the pore geometry, and the onset of this regime is accentuated with the increasing values of the Weissenberg number and decreasing values of the nonlinear VCM model parameter ξ. Apart from the flow pattern, a detailed discussion on the distribution of the wormlike micellar concentration, principal stress difference, apparent relative viscosity, etc., is also presented. Finally, a good qualitative agreement (in terms of the flow pattern) has been found between the present simulations and the corresponding experiments.

14.	[Impromptu Rendezvous Based Multi-threaded Algorithm for Shortest Lagrangian Path Problem on Road Networks](#) K Vishwakarma, VMV Gunturi - International Conference on Algorithms and Architectures for Parallel Processing: Part of the Lecture Notes in Computer Science book series (LNCS, volume 11944), 2019 **Abstract:** Input to the shortest lagrangian path (SLP) problem consists of the following: (a) road network dataset (modeled as a time-varying graph to capture its temporal variation in traffic), (b) a source-destination pair and, (c) a departure-time (tdeptdep). Given the input, the goal of the SLP problem is to determine a fastest path between the source and destination for the departure-time tdeptdep (at the source). The SLP problem has value addition potential in the domain of urban navigation. SLP problem has been studied extensively in the research literature. However, almost all of the proposed algorithms are essentially serial in nature. Thus, they fail to take full advantage of the increasingly available multi-core (and multi-processor) systems. However, developing parallel algorithms for the SLP problem is non-trivial. This is because SLP problem requires us to follow Lagrangian reference frame while evaluating the cost of a candidate path. In other words, we need to relax an edge (whose cost varies with time) only for the time at which the candidate path (from source) arrives at the head node of the edge. Otherwise, we would generate meaningless labels for nodes. This constraint precludes use of any label correcting based approaches (e.g., parallel version of Delta-Stepping at its variants) as they do not relax edges along candidate paths. Lagrangian reference frame can be implemented in label setting based techniques, however, they are hard to parallelize. In this paper, we propose a novel multi-threaded label setting algorithm called IMRESS which follows Lagrangian reference frame. We evaluate IMRESS both analytically and experimentally. We also experimentally compare IMRESS against related work to show its superior performance.
15.	[Maximum Weighted Edge Biclique Problem on Bipartite Graphs](#) A Pandey, G Sharma, N Jain - CALDAM 2020: Algorithms and Discrete Applied Mathematics: Part of the Lecture Notes in Computer Science book series (LNCS, volume 12016), 2020 **Abstract:** For a graph G, a complete bipartite subgraph of G is called a biclique of G. For a weighted graph $G=(V,E,w)$, where each edge $e \in E$ has a weight $w(e) \in R$, the Maximum Weighted Edge Biclique (MWEB) problem is to find a biclique H of G such that $\sum_{e \in E(H)} w(e)$ is maximum. The decision version of the MWEB problem is known to be NP-complete for bipartite graphs. In this paper, we show that the decision version of the MWEB problem remains NP-complete even if the input graph is a complete bipartite graph. On the positive side, if the weight of each edge is a positive real number in the input graph G, then we show that the MWEB problem is $O(n2)$-time solvable for bipartite permutation graphs, and $O(m+n)$-time solvable for chain graphs, which is a subclass of bipartite permutation graphs.
16.	[Normalized unit groups and their conjugacy classes](#) S Kaur, M Khan - Proceedings-Mathematical Sciences, 2020 **Abstract:** Let $G = H \times A$ be a finite 2-group, where H is a non-abelian group of order 8 and A is an elementary abelian 2-group. We obtain a normal complement of G in the normalized unit group $V(FG)$ and in the unitary subgroup $V*(FG)$ over the field F with 2 elements. Further, for a finite field F of characteristic 2, we derive class size of elements of $V(FG)$. Moreover, we provide class representatives of $V*(F H)$.

17.	Note: A Novel Virtual Guidance based Emergency Treatment using Low Cost Drone Network SJ Badri, VSRT Reddy, VBR Chintakunta, SR Kamini - AIMS '20: Proceedings of the 1st ACM Workshop on Autonomous and Intelligent Mobile Systems, 2020 **Abstract:** Unmanned Aerial Vehicles (UAV) or Drones have been developing in an exponential rise within a few decades, and they represent outstanding progress in several applications. Applications like human reach are either severe or venturous, particularly within the tedious and risky activities with advanced technology. However, we have stepped towards human health emergency cases like sudden strokes, natural disasters, and they need necessary treatment. A drone network with a high-speed that delivers emergency supplies to the location range with an adequate time constant. The primary objective of this work is to develop a drone system that will fly autonomously, travelling to multiple locations through the utilization of a Global positioning system (GPS) module with a minimum time constant. The second objective of this work is the installation of medical accessories for health care. Therefore, we can use a drone for medical assistance in emergency cases.
18.	Preventing Security and Privacy Attacks in WBANs A Vyas, S Pal - Handbook of Computer Networks and Cyber Security, 2020 **Abstract:** Sensors and radio channels have made remote health monitoring easier with the use of wireless body area networks (WBANs). WBANs use bio-sensors, implanted on/inside the human body, to collect real-time health readings. These sensors collect data wirelessly and then send it to medical server via wireless communication channels. Human health readings are of great importance and wireless channels are not always secure. This makes security and privacy disquiet in WBANs. Sensor nodes are the most common target of an intruder in WBANs. Intruder can also attack the communication channels and medical server of WBANs. Therefore, WBAN needs prevention while sending sensed information to the health care monitoring system. We also need to maintain confidentiality while transmitting the data to the server. In this chapter, we discuss various types of possible attacks in WBANs and summarized different lightweighted security methods proposed for resource constraint WBANs. We thoroughly explained how channel characteristics and human body features could be exploited to identify intruder in WBANs without using complex encryption. Additionally, the chapter briefly review methods for generating symmetric keys and exchanging messages over insecure channels in cloud assisted WBANs.
19.	Regioselective Brønsted Acid Catalyzed Annulation of Cyclopropane Aldehydes with N'-Aryl Anthranil Hydrazides: Domino Construction of Tetrahydropyrrolo [1, 2-a] quinazolin-5(1H)ones P Singh, N Kaur, P Banerjee - The Journal of Organic Chemistry, 2020 **Abstract:** A highly regioselective synthesis of tetrahydropyrrolo[1,2-a]quinazolin-5(1H)one derivatives was achieved by reacting cyclopropane aldehydes with N'-aryl anthranil hydrazides in the presence of PTSA (p-toluene sulphonic acid). The transformation involves domino imine formation and intramolecular cyclization to form 2-arylcyclopropyl-2,3-dihydroquinolin-4(1H)-one, followed by nucleophilic ring opening of the cyclopropyl ring to form desired tetrahydropyrrolo[1,2-a]quinazolin-5(1H)one in good to excellent yield with complete regioselectivity. This protocol tolerates a great variety of functional groups and thus provides a simple and step efficient method for pyrroloquinazolinones synthesis.

20.	Residual stress inclusion in the incrementally formed geometry using Fractal Geometry Based Incremental Toolpath (FGBIT) HK Nirala, A Agrawal - Journal of Materials Processing Technology, 2020 **Abstract:** Single Point Incremental Sheet Forming (SPISF) is a well-known flexible alternative to conventional generative manufacturing processes. In SPISF, the geometry to be formed is fragmented into series of 2D slices and the plastic deformation is achieved through layer by layer movement of a Numerically Controlled (NC), hemispherical or ball end forming tool. The whole plastic deformation is the sum of all localized strains developed during each increment. Spiral, constant z incremental toolpaths, and their variants are common conventional toolpaths for SPISF. Several researchers have investigated these toolpaths extensively. Fractal Geometry Based Incremental Toolpath (FGBIT) is a recently developed toolpath for SPISF that improves the process formability and stress distribution. Unlike conventional toolpaths, FGBIT deforms the base region of the formed geometry which induces work hardening and residual stresses into the work piece. This may lead to the forming of high strength components. The residual stress distribution over the base region of the formed component (square cup) has been investigated in this study. Further, a comparison based on residual stress distribution between FGBIT and conventional incremental toolpaths is presented. Residual stresses have been measured by using nanoindentation technique. Pile up generation near the periphery of the indent is investigated for conventional and FGBIT based toolpaths. It has been observed from the experimental results that, the strength of the formed component increases due to induced compressive surface residual stresses while using FGBIT hence, metal components with high fatigue life and better strength-to-weight ratio can be formed.
21.	Sensitivity of nuclear matrix elements of $0\nu\beta\beta$ of 48Ca to different components of the two-nucleon interaction S Sarkar, P Kumar, K Jha, PK Raina - Physical Review C, 2020 **Abstract:** In the present work, we examine the sensitivity of nuclear matrix elements (NMEs) for light neutrino-exchange mechanism of neutrinoless double beta decay ($0\nu\beta\beta$) of 48Ca to the central, spin-orbit, and tensor components of two-nucleon interaction. The NMEs are calculated in the nuclear shell-model framework in fp-model space using frequently used GXPF1A interaction and a new effective interaction named GX1R of pf shell. The decomposition of the shell-model two-nucleon interactions into their individual components is performed using spin-tensor decomposition. The NMEs are calculated in closure approximation by using optimal value of the closure energy. The results shows that the total NMEs calculated with the central component of the interactions are of positive sign. By adding spin-orbit part to central part of the interactions, sign of the total NMEs gets change, and in absolute value, NMEs decreases by about 15–18%. Sign change in total NMEs are again seen by adding tensor part to the central+spin−orbit part of the interactions. Similar trends of sign change are also observed for Fermi, Gamow-Teller, and tensor matrix elements. Thus we infer that SO and T part mostly cancel the effects of each other in NMEs calculations. For both the interactions, the total NMEs calculated with the C part is found to be 20% enhanced as compared to the NMEs calculated with the total interactions. With new GX1R interaction, there is about 1–3% increments in the total NMEs as compared to NMEs with GXPF1A interaction. This increments comes from the modifications of isospin T=1 tensor force two-nucleon matrix elements to bring the characteristic properties of tensor force into the GX1R interaction.

22.	[Transient growth and symmetrizability in rectilinear miscible viscous fingering](#) TK Hota, M Mishra - Journal of Engineering Mathematics, 2020 **Abstract:** The influence of dispersion or equivalently of the Péclet number (Pe) on miscible viscous fingering in a homogeneous porous medium is examined. The linear optimal perturbations maximizing finite-time energy gain is demonstrated with the help of the propagator matrix approach based non-modal analysis (NMA). We show that onset of instability is a monotonically decreasing function of Pe and the onset time determined by NMA emulates the non-linear simulations. Our investigations suggest that perturbations will grow algebraically at early times, contrary to the well-known exponential growth determined from the quasi-steady eigenvalues. One of the over-arching objective of the present work is to determine whether there are alternative mechanisms which can describe the mathematical understanding of the spectrum of the time-dependent stability matrix. Good agreement between the NMA and non-linear simulations is observed. It is shown that within the framework of L2L2-norm, the non-normal stability matrix can be symmetrizable by a similarity transformation and thereby we show that the non-normality of the linearized operator is norm dependent. A framework is thus presented to analyze the exchange of stability which can be determined from the eigenmodes.
23.	[""Turn-On" Sensing Behaviour of an In Situ Generated Fluorescein-Based Probe and Its Preferential Selectivity of Sodium Hypochlorite over *tert*-Butyl Hydroperoxide in Lung Adenocarcinoma Cells"](#) N Sandhu, S Saproo, S Naidu, AP Singh, K Kumar… - ChemistrySelect, 2020 **Abstract:** Reactive Oxygen species (ROS) are well known for their oxidizing behaviour but it differs in fluorescein derivatives chemistry. With t-BuOOH, the probe F shows its unique turn-off sensing (A), while with NaOCl probe shows turn-on sensing property (B). In this study, it was observed that in situ generated species formed by the reaction of probe (F) with t-BuOOH is a unique molecule, having high turn-on behaviour in presence of sodium hypochlorite (≈500 times). Further, fluorescence microscopy imaging using adenocarcinoma cells, A549 cells revealed that in-situ generated molecule, could be used as an efficient fluorescent probe for detecting NaOCl in living cells.